The Role of Nucleobase Carboradical and Carbanion on DNA Lesions: A Theoretical Study

Ru bo Zhang[†,‡] and Leif A. Eriksson*[,†]

Department of Natural Sciences and Örebro Life Science Center, Örebro University, 701 82 Örebro, Sweden, and School of Science and the Institute for Chemical Physics, Beijing Institute of Technology, Beijing 100081, China

Received: June 9, 2006; In Final Form: September 14, 2006

DNA base release induced by H and OH radical addition to thymine and their corresponding electron adducts is studied at the DFT B3LYP/6-31+G(d,p) level in gas phase and in solution. H atom transfer after radical formation from C2′ on the sugar to the C6 site on the base is shown to be prohibited for the radical species. Their corresponding electron adducts, albeit minor events in cellular systems, show excellent capabilities to proton transfer from C2′ on the sugar to the C6 site on the base. The barriers for subsequent *N*-glycosidic bond dissociation range from 0.1 to 1.6 kcal mol^{-1} at the B3LYP level and around 5 kcal mol^{-1} using the BB1K functional, implying that these reactions can serve as a source to abasic sites. Analysis of bond dissociation energies show that all the reactions are exothermic, which is consistent with the changes in *N*-glycosidic bond lengths during the proton-transfer reactions. Bulk solvation plays a reverse influence on proton transfer and the bond rupture reactions. Molecular orbitals, NPA charges, and electron affinities are calculated to shed further light on the properties leading up to the intramolecular reactions.

1. Introduction

In living cells, the DNA molecule is the primary target of ionizing radiation.[1] The mechanisms involved in radiation damage to DNA are often highly complex. Despite their importance, some questions still remain to be answered in order to fully understand the damage processes of DNA and their implications in the form of altered bases, altered sugar moieties, base release, strand breaks, and DNA−DNA or DNA−protein cross-links;[2,3] changes that can contribute to a number of pathological conditions including cancer, neurodegeneration, and natural processes of aging.[4] Most of these lesions are repaired by base excision repair (BER) and nucleotide excision repair (NER) through the various DNA repair enzymes.[5]

It is noteworthy that the initial reactive species, such as free electrons, H-atoms, and OH radicals, largely originate from radiolysis of the surrounding aqueous medium and from normal cell metabolism.[6,7] To date, much work has been devoted to unveil the effects and mechanisms of radiation in DNA lesion formation.[8] OH radical attack on the bases primarily results in addition to the electron-rich double bonds.[9−12] Of relevance to the current study, the hydroxyl radical is known to react with thymine, either by addition to the C5═C6 double bond or by abstraction of a hydrogen atom from the C5 methyl group, with addition to C5 being the major pathway.[8] For H atom addition, formation of the 5,6-dihydro-5-thymyl radical is preferred over the 5,6-dihydro-6-thymyl radical from both thermodynamic and kinetic points of view, although the relative energy between the two products is only 3.1 kcal/mol.[13] A competing set of reactions is initiated by H atom abstraction from the sugar moiety by the OH radical. These depend on the C−H bond strength and lead to alteration of the sugar moiety and subsequent rearrangements, leading to base release and/or strand break.[14,15]

The radical intermediates formed have very versatile properties. The direct effects of solvated or low-energy electrons has recently been given much attention from experimental and theoretical perspectives, in particular, regarding electron impact induced scission of the nucleic acid strand.[16−23] The cleavage modes are mainly associated with the strengths of the C′−O and C′−N (*N*-glycosidic) bonds, and relatively high activation energy (18.9 kcal/mol for $dT^{\bullet}$ and 20.6 kcal/mol for $dC^{\bullet}$) for *N*-glycosidic bond rupture has been estimated.[22] Rupture of either the 3′ or the 5′ C−O sugar−phosphate σ-bond has been reported at the HF and DFT levels to have an energy barrier of about 10 kcal/mol and with the barriers strongly dependent on solvation included.[24] It is generally accepted that nucleobase-radical adducts contribute to strand break.[25−27] The exact mechanism is, however, uncertain to date. Electron spin resonance (ESR) results have indicated this to be a slow process,[28] with the rate-limiting step suggested to involve hydrogen atom abstraction from an adjacent nucleotide (path A in Scheme 1).[29] This process has also been proposed to take the route by way of initial protonation of the radical adduct, followed by reversible dehydration/hydration to form the 6-hydroxy adduct radical, intramolecular H-transfer, and strand scission (path B, shown schematically in Scheme 1).[30] The mechanism involving intramolecular hydrogen atom abstraction (path C), as well as the protonation/dehydration pathway B, was thought to be less important in the biopolymer due to the stability of the nucleobase-radical adduct.[31] Our theoretical studies have also indicated that the intramolecular hydrogen abstraction (C) is a slow process, although thermodynamically favored in a nonpolar environment. These observations were again mainly attributed to the high stability of the radical adducts.[32]

* Corresponding author. E-mail: leif.eriksson@nat.oru.se.
† Örebro University.
‡ Beijing Institute of Technology.

10.1021/jp063605b CCC: $33.50
Published on Web 10/27/2006

SCHEME 1

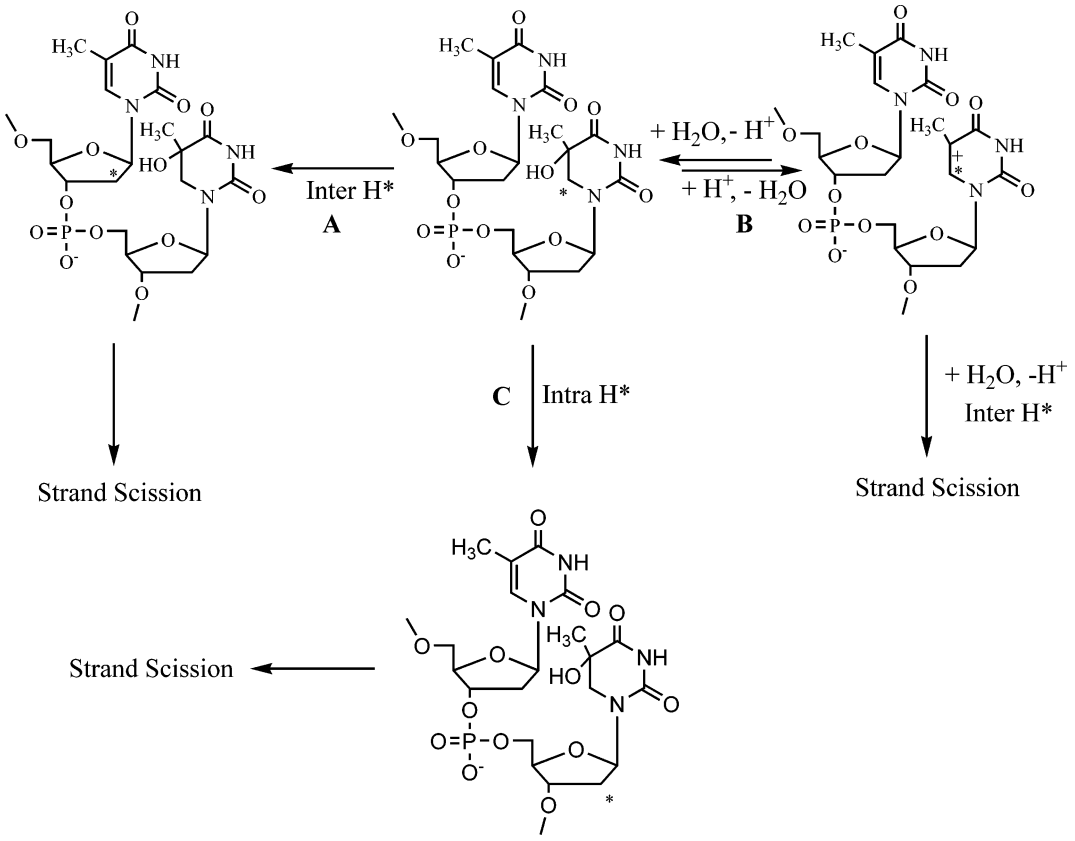

It is well established that the OH′ and H′ radical adducts of the pyrimidines can be reducing and/or oxidizing.[33,34] *N*-glycosidic bond rupture has been proposed to be caused by the cationic C6 lesion, arising as a result of one-electron removal of the 5,6-dihydro-6-thymyl radical.[35] The capture of an additional electron by the cytosine N3−H atom radical adduct led to the automatic rupture of the C3′−O(P) bond.[36] The work reported herein primarily refers to thymidine 5′-monophosphate (5′dTMP, cf. Scheme 2), which is employed to model the 5′-terminal of the DNA strand. Given the complex and asymmetric local environment, both "back" and "front" attack at the C5 site of the base by the OH and H radicals are considered. In particular, the processes of the carbon-centered H atom and proton transfer from C2′ on the sugar moiety to C6 on the radical-modified thymine base are explored in detail at the density functional theory (DFT) framework. The bond dissociation energy (BDE) of the C3′−O(P) and C1′−N1 (glycosidic bond) bonds are calculated in order to investigate possible cleavage modes in DNA under the oxidative and reductive stress.

SCHEME 2

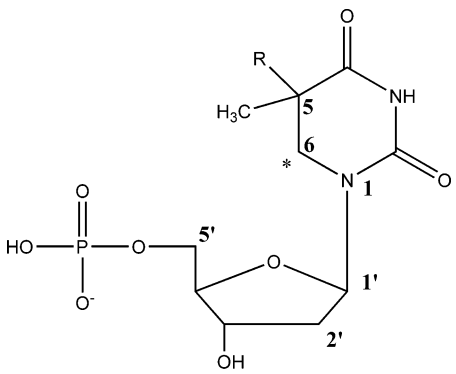

R = H or OH

2. Methodology

The geometries of the different systems were optimized at the hybrid Hartee−Fock density functional theory level B3LYP,[37,38] in conjunction with the 6-31+G(d,p) basis set. Frequency calculations were performed at the same level of theory to confirm the correct nature of the stationary points. The charges obtained from natural population analysis (NPA) were determined by means of the natural bond orbital (NBO) theory.[39] Bulk solvation effects were considered using the integral equation formalism of the polarized continuum model (IEF−PCM),[40] with dielectric constants $\epsilon = 4.3$ and $\epsilon = 78.4$, respectively. All calculations were performed using the Gaussian 03 package.[41] Atomic labeling used in the text and tables throughout refers to Scheme 2. The DNA strand was truncated by hydrogen atoms at the C3′OH and the C5′−$OP(O)_2$−OH ends, and the phosphate group was kept negatively charged to ensure an appropriate environment. The use of a negatively charged phosphate group proved to be crucial to the results obtained, as will be discussed below.

To investigate low barriers toward *N*-glycosidic bond cleavage for electron adducts, additional single-point calculations at the BB1K/6-31+G(d,p) level were conducted.[42,43] The hybrid meta-GGA functional BB1K is reported as one of the most accurate for barrier heights among the new generation of improved DFT functionals.[43]

3. Results and Discussions

3.1. H Atom Transfer Initiated by H and OH Radical Adducts to 5′dTMP. As previously noted, •H and •OH addition

TABLE 1: Selected Geometrical Parameters of Radical-5′DTMP and Their Electron Adducts Obtained at the B3LYP/6-31+G(d,p) Level

radical	TH1′	TH2′	TH3′	TH1	TH2	TH3
C5C6	1.496	1.512	1.533	1.493	1.511	1.531
N1C1′	1.467	1.469	1.461	1.47	1.470	1.463
H2′C6	2.629	1.358	1.092	2.73	1.356	1.089
C5′O(P)	1.417	1.414	1.418	1.417	1.415	1.418
anion	ATH1′	ATH2′	ATH3′	ATH1	ATH2	ATH3
C5C6	1.514	1.521	1.532	1.502	1.520	1.534
N1C1′	1.437	1.495	1.534	1.442	1.505	1.536
H2′C6	2.655	1.419	1.101	2.857	1.419	1.089
C5′O(P)	1.421	1.423	1.428	1.422	1.422	1.429
radical	TOH1′	TOH2′	TOH3′	TOH1	TOH2	TOH3
C5C6	1.500	1.512	1.545	1.499	1.525	1.543
N1C1′	1.466	1.466	1.455	1.481	1.479	1.488
H2′C6	2.639	1.363	1.100	3.107	1.357	1.087
C5′O(P)	1.422	1.419	1.424	1.42	1.422	1.419
anion	ATOH1′	ATOH2′	ATOH3′	ATOH1	ATOH2	ATOH3
C5C6	1.460	1.497	1.524	1.485	1.506	1.535
N1C1′	1.437	1.510	1.565	1.444	1.496	1.502
H2′C6	2.716	1.370	1.099	2.621	1.390	1.093
C5′O(P)	1.421	1.423	1.426	1.421	1.423	1.427

TABLE 2: B3LYP/6-31+G(d,p) Reaction Energies and Activation Barriers (in kcal/mol) for the Intramolecular H Abstraction Reactions

radical		TH1′ → 3′	TH1 → 3	TOH1′ → 3′	TOH1 → 3
$\Delta E^{\ddagger a}$	vacuum	30.4	29.1	34.7	35.9
	$\epsilon = 4.3$	28.0	27.2	34.1	34.8
	$\epsilon = 78.4$	27.4	27.0	33.6	34.1
ΔE^{b}	vacuum	6.1	6.8	6.5	9.6
	$\epsilon = 4.3$	4.6	6.0	4.8	8.5
	$\epsilon = 78.4$	3.3	4.9	2.4	5.8

[a] Activation energies. [b] Reaction energies.

in 5′dTMP occurs primarily at the C5 site. Two cases are considered: radical attack from back ("primed") and front ("unprimed") at the C5 site of the base, TH1′ (TOH1′) and TH1 (TOH1), respectively (cf. Scheme 2). The TH1′ and TH1 radicals have almost the same stability. The energy difference of the two radicals TOH1′ and TOH1 is 2.3 kcal mol^{-1} in favor of the "front" adduct TOH1 due to a more favorable interaction between the phosphate group and the C5OH group and between the sugar and the radical site. The C5−C6 distance is 1.49−1.50 Å, characteristic of a single bond, as shown in Table 1. The C6 site is slightly pyramidal with the sum of the angles ∠C5C6N1 + ∠C5C6H6 + ∠H6C6N1 ranging from 355.6° in TH1′ to 357.6° in TOH1′, which is attributed to the radical (•H and •OH) addition to C5, through which the resulting unpaired electron becomes mainly localized on C6. Among the H atoms of the 2-deoxyribose moiety, H2′ is the one closest to the radical center C6 at a distance ranging from 2.62 to 3.10 Å. Strand breakage and/or base release has been attributed to H2′ abstraction by the C6 radical center[26] and is the primary reaction studied herein.

The energetic profile for the radical-induced H-abstraction process is listed in Table 2. The activation barrier for H2′ atom transfer to C6 ranges from 29.1 to 36.0 kcal mol^{-1} for the TH1-(′) → TH3(′) and TOH1(′) → TOH3(′) reactions in the gas phase, with the •OH adducts having the higher activation energies. The reactions are slightly endothermic, with reaction energies from 6.0 to 10.0 kcal mol^{-1}. The results show that the reactions are not favored, neither kinetically nor thermodynamically. Bulk solvation contributes by lowering the barriers and reducing reaction energies, but the changes are too small to alter reaction characteristics. The forbidden reactions are largely attributed to the significant stabilities of reactant adducts, as also noted in a recent study of 3′dTMP.[32]

3.2. Proton Transfer Initiated by the 5′dTMP Carbanion. As noted in the Introduction, the radical adducts are oxidizing and could capture an excess electron from the surroundings to form the closed-shell dianionic species (the first electron already present on the negatively charged phosphate group in the current systems). In the dianions ATH1′ (backward attack) and ATH1 (forward attack), corresponding to the reduced forms of the TH1′ and TH1 radical adducts, respectively, ATH1′ is slightly more stable, by 2.2 kcal mol^{-1}, than ATH1. In both cases, the C5C6, H2′C6, and C5′O(P) distances are extended and N1C1′ distances contracted relative to the parent compounds TH1 and TH1′. The negative charge is mainly localized on the phosphate group and in part on the modified bases. NBO charge analysis, presented in Table 3, reveals that the radical-modified bases carry net negative charges of −0.28 e$^-$ (TH1′) and −0.31 e$^-$ (TOH1′), respectively. For the ATH1 and ATH1′ dianions, the sp^3 hybridized C6 hosts a negative charge up to −1.20 e$^-$. The pyramidality at C6 is enhanced in the dianions due to the increased occupancy of the lone pair on C6, as illustrated by the sum of the angles ∠C5C6N1 + ∠C5C6H6 + ∠H6C6N1 (326.5° in ATH1′ and 337.8° in ATH1). The charges on the 2-deoxyribose and phosphate groups are essentially unaltered relative to the radical species. Thus, two negatively charged centers are formed, the modified base and the phosphate group, causing these to repel. This in part explains the different configurations between nucleobase-radicals and their electronic adducts.

The adiabatic electronic affinities (AEA) of the radical adducts (TH1(′) and TOH1(′)) are presented in Table 4. In gas phase, the intermediates become unstable when they capture an excess electron. The AEA values of TH1(′) are more negative than the ones of TOH1(′). The AEA become positive due to the influence of bulk solvation, which shows that the parent radical adducts are oxidizing in solutions. In addition, increasing the solvent polarity results in enhanced dianion stability, which is explained in terms of the two charged centers and large dipole moments.

As illustrated in Figures 1 and 2, intramolecular proton transfer can occur from C2′ of the 2-deoxyribose to C6 of the base adducts, as the latter carry a significant portion of the excess negative charge. In the transition states (TS), the transferred protons are found at distances 1.419 Å to C6 and 1.449 Å to C2′ in ATH2′ as well as in ATH2. For ATOH2(′), the TS's occur later than in ATH2(′), as manifested in the shorter distance of the transferred proton to C6 and longer distances to C2′. The C5C6 and N1−C1′ distances are extended by 0.03 and 0.05 Å, respectively, whereas the C5′−O(P) bond length remains essentially unchanged.

The activation barrier is estimated to be 12.5 kcal mol^{-1} for ATH1′ → ATH3′ in gas phase, which is considerably lower than the 30.4 kcal/mol barrier obtained for the H atom abstraction reaction TH1′→TH3′ of the parent radical adduct system, as shown in Table 5. There is very little influence from bulk solvation. The proton-transfer barrier is comparable to that seen for the $(H_3C\cdots H\cdots CH_3)^{\ddagger}$ reaction in aqueous solution.[44] For the ATH1 → ATH3 reaction, an even lower barrier is found, 5.8 kcal mol^{-1}. The results show that the local surrounding governs the proton-transfer reaction in a stereoselective way, that is, the proton transfer is much preferred in the "forward"

TABLE 3: NPA Charge Distribution of Radical Anions and Their Adiabatic Closed-Shell Electron Adducts in Vacuum on Base (B), Sugar (S), and Phosphate Group (P)

	TH1′			TH3′			TH1			TH3		
	B	S	P	B	S	P	B	S	P	B	S	P
radical	−0.28	0.53	−1.25	−0.26	0.51	−1.25	−0.28	0.54	−1.25	−0.26	0.51	−1.25
anion[a]	−1.18	0.45	−1.27	−0.41	−0.31	−1.28	−1.18	0.45	−1.27	−0.40	−0.32	−1.29
	TOH1′			TOH3′			TOH1			TOH3		
	B	S	P	B	S	P	B	S	P	B	S	P
radical	−0.31	0.53	−1.23	−0.29	0.51	−1.21	−0.34	0.55	−1.25	−0.32	0.54	−1.22
anion[a]	−1.19	0.46	−1.27	−0.38	−0.34	−1.28	−1.17	0.45	−1.27	−0.41	−0.30	−1.29

[a] Adiabatic species.

TABLE 4: Adiabatic Electronic Affinities (in eV) Obtained at the B3LYP/6-31+G(d,p) Level[a]

	TH1′	TH3′	TH1	TH3
vacuum	−1.37	−0.83	−1.46	−0.87
$\epsilon = 4.3$	1.75	2.26	1.65	2.25
$\epsilon = 78.4$	2.84	3.12	2.75	3.10
	TOH1′	TOH3′	TOH1	TOH3
vacuum	−1.17	−1.02	−1.20	−1.22
$\epsilon = 4.3$	1.92	2.07	1.86	1.98
$\epsilon = 78.4$	3.04	2.91	2.93	2.96

[a] Negative value indicates an endothermic process.

radical adduct ATH1′ than in the "backward" form. In addition, the ATH1 → ATH3 reaction is slightly more favored in a nonpolar solvent (barrier 5.2 kcal mol^{-1}), but somewhat less so in aqueous medium.

For the proton-transfer products, the C5C6, N1C1′, and C5′O-(P) bond lengths increase. In particular, the *N*-glycosidic bonds are elongated from 1.437 Å in ATH1′ to 1.534 Å in ATH3′ and from 1.442 Å in ATH1 to 1.536 Å in ATH3, implying that *N*-glycosidic bond rupture might be enhanced in the dianionic state of 5′dTMP. The proton-transfer reactions involving the electron adducts of 5′dTMP−H atom complexes are exothermic by 6.9 kcal mol^{-1} in gas phase, 3.1 kcal mol^{-1} in aqueous medium, and 7.7 kcal mol^{-1} in the nonaqueous medium.

For the electron adducts involving the 5′dTMP−OH radical complexes, the barriers for proton-transfer reactions from C2′ to C6 remain relatively high and are essentially inaccessible. The barrier of the ATOH1 → ATOH3 reaction is 18.0 kcal mol^{-1} in nonaqueous medium and 19.3 kcal mol^{-1} in gas phase. The values are lower by 7.0 kcal mol^{-1} than those observed for the ATOH1′ → ATOH3′ reaction. The reactions are

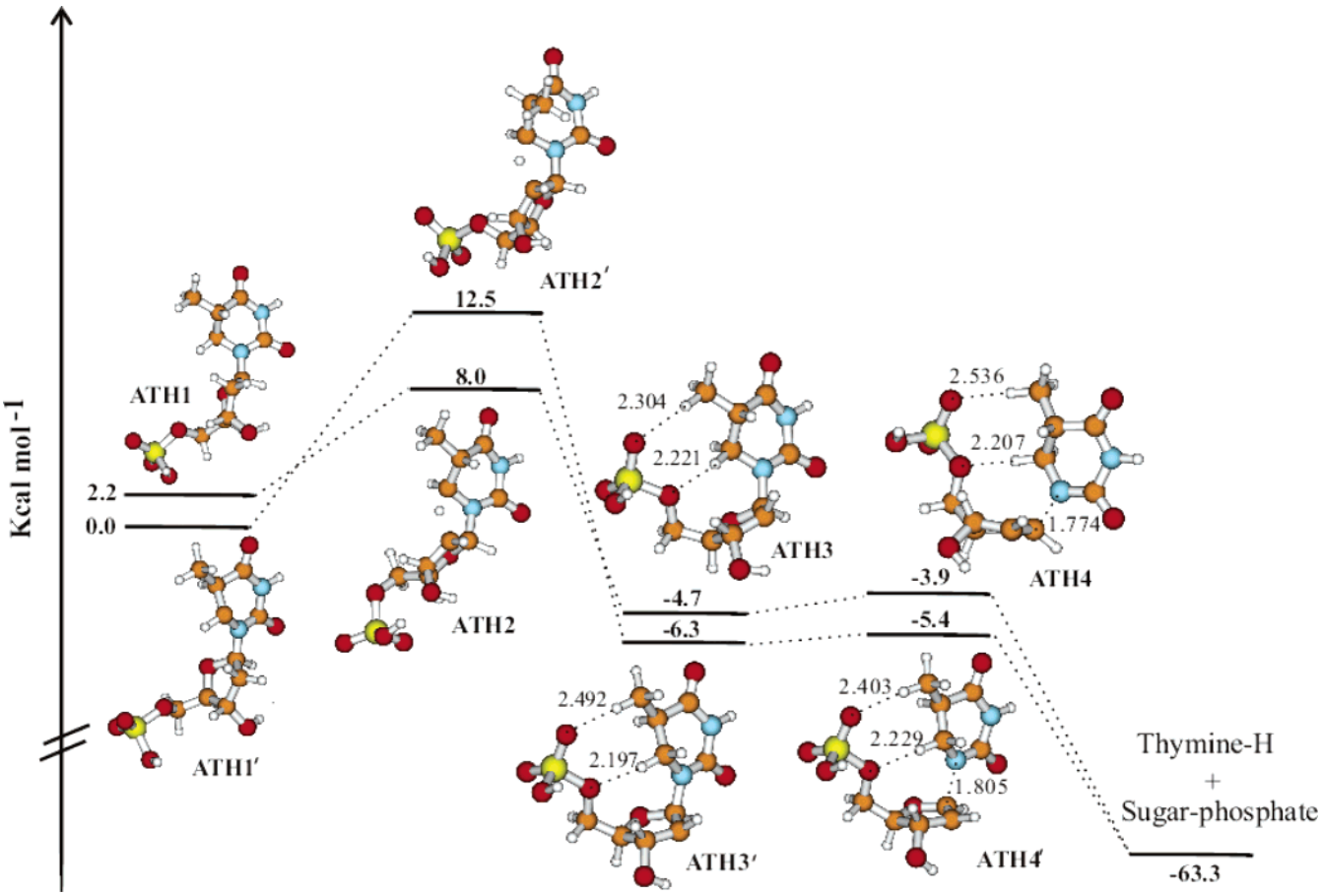

Figure 1. Energy profiles and selected geometrical parameters of the stationary structures along the proton transfer and the *N*-glycosidic bond rupture reactions ATH1(′) → ATH3(′) → decomposed species, obtained at the (U)B3LYP/6-31+G(d,p) level.

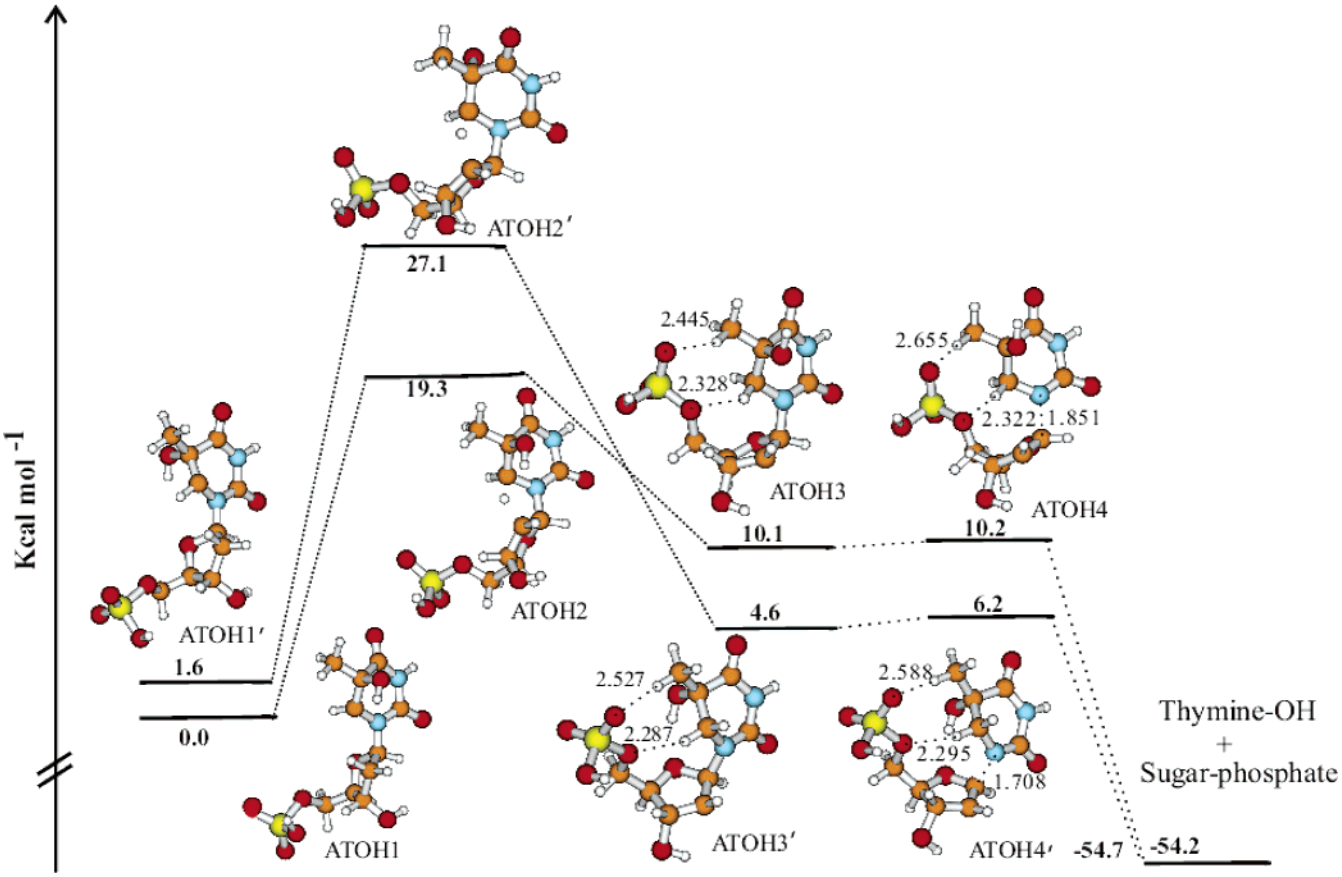

Figure 2. Energy profiles and selected geometrical parameters of the stationary structures along the proton transfer and the *N*-glycosidic bond rupture reactions ATOH1(′) → ATOH3(′) → decomposed species, obtained at the (U)B3LYP/6-31+G(d,p) level.

TABLE 5: B3LYP/6-31+G(d,p) Reaction Energies and Activation Barriers (in kcal/mol) for Proton Transfer and *N*-glycosidic Bond Cleavage of the Electron Adducts[a]

proton transfer		ATH1′ → 3′	ATH1 → 3	ATOH1′ → 3′	ATOH1 → 3
$\Delta E^{\ddagger b}$	vacuum	12.5	5.8	25.5	19.3
	$\epsilon = 4.3$	12.0	5.2	25.1	18.0
	$\epsilon = 78.4$	14.7	11.3	26.5	18.6
ΔE^{c}	vacuum	−6.3	−6.9	3.0	10.1
	$\epsilon = 4.3$	−7.1	−7.7	1.4	6.0
	$\epsilon = 78.4$	−3.2	−3.1	5.5	5.1
bond rupture		ATH3′ → prod	ATH3 → prod	ATOH3′ → prod	ATOH3 → prod
$\Delta E^{\ddagger b}$	vacuum	0.9 (5.0)	0.8 (6.6)	1.6 (5.5)	0.1 (3.5)
	$\epsilon = 4.3$	3.4	3.0	3.8	2.2
	$\epsilon = 78.4$	4.0	3.0	4.3	2.6
ΔE^{c}	vacuum	−57.0	−58.6	−59.3	−64.9
	$\epsilon = 4.3$	−51.7	−53.3	−34.0	−37.8
	$\epsilon = 78.4$	−29.8	−31.6	−32.0	−32.3

[a] Values in parenthesis are from BB1K/6-31+G(d,p) calculations. [b] Activation energies. [c] Reaction energies.

furthermore endothermic, by between 1.4 and 10.1 kcal mol^{-1}, depending on the medium.

The differences seen for the proton-transfer reactions involving the electron adducts of the 5′dTMP−H and 5′dTMP−OH radical complexes depend on the basicity of the negatively charged center C6 and the acidity of H2′ of 2-deoxyribose and their local environments. As presented in Figure 3, NBO charge analysis shows that C5 carries a significant negative charge, −0.4 e^{-} in the electron adducts of 5′dTMP−H, much more negative than the corresponding values for the electron adducts of 5′dTMP−OH (+0.08 e^{-}), which are affected by the neighboring OH. The larger amount of negative charge in turn favors the localization of negative charge at C6, which thus behaves as a stronger base. The excess negative charge on C5,

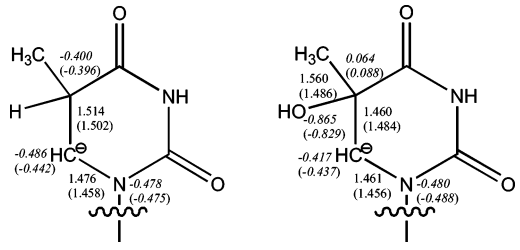

Figure 3. Selected parameters of NPA charges (italics) and bond lengths (in Å) in ATH1(′) and ATOH1(′).

C6, and N1 of the electron adducts of 5′dTMP−H induces repulsion leading to elongated C5C6 and C6N1 bonds than what is seen in the corresponding electron adducts of 5′dTMP−OH.

The C2′H2′ bonds are also polarized by the local environment, although their differences are relatively small; the C2′H2′ bond lengths range from 1.092 Å in ATH1′ and ATOH1′ to 1.093 Å and 1.095 Å in ATOH1 and ATH1, respectively. The symmetrical and unsymmetrical stretching frequencies of the two H2′ atoms are centered around 3130 and 3070 cm^{-1}, respectively, and the changes are within 10 cm^{-1}. We hence conclude that the proton-transfer reactions are more facile in the electron adducts of the 5′dTMP−H radical complexes than in the electron adducts of 5′dTMP−OH, mainly due to the stronger basicity of C6 in the former.

3.4. Carbanion-Induced Bond Scission. The proton-transfer reactions result in the sp^3 hybridized C2′-centered sugar anion, depicted in Figures 1 and 2. NBO analysis (Table 3) shows that the negative charge is transferred from the radical-altered nucleobase to 2-deoxyribose in all the ATH1(′) → ATH 3(′) and ATOH1(′) → ATOH3(′) reactions, resulting in an increased negative charge on the sugar by ca. −0.81 to −0.84 e^-. The charges on the phosphates are unchanged. AEA calculations show that the dianions ATH3(′) and ATOH3(′) are more stable than ATH1(′) and ATOH1(′) in gas as well as nonaqueous phases. The notable increases of *N*-glycosidic bond lengths in these reactions illustrate the possibility of the bond rupture and base release.

Markedly low barriers in order to break the *N*-glycosidic bonds, 0.8 (0.9) and 0.1 (1.6) kcal mol^{-1} in gas phase, are found for ATH3(′) and ATOH3(′) at the B3LYP/6-31G+(d,p) level of theory; see Table 5. For the heterolytic dissociation products, the two negative charges are mainly localized on the phosphate (−1.27 e^-) and the modified base (−0.54 e^-), respectively. The total bond dissociation energies (BDE) of the *N*-glycosidic bonds are in gas phase −57.0 kcal mol^{-1} (ATH1′), −58.6 kcal mol^{-1} (ATH1), −59.3 kcal mol^{-1} (ATOH1′), and −64.9 kcal mol^{-1} (ATOH1), respectively. Because of the cleavage of the N1−C1′ bond, new double bonds are formed between C1′ and C2′ on the sugar and N1 and C2 on the modified base, which provides enhanced stability to the products. The effects of bulk solvation are slightly unfavorable to the dissociation of the *N*-glycosidic bonds, but cannot change the reaction properties.

To verify the small/negligible barriers found for the *N*-glycosidic bond rupture, single-point calculations were performed in vacuo, using the highly accurate hybrid meta-GGA BB1K,[42,43] in conjunction with the same basis set. The results are given in parentheses in Table 5. As seen, the BB1K calculations predict the barriers to increase to between 3.5 and 6.6 kcal mol^{-1} and are expected to be similar, or possibly up to 2 kcal mol^{-1} higher, in the presence of bulk solvation. The anionic base release reaction is hence expected to proceed very rapidly also based on the BB1K data, albeit with slightly more hindered kinetics.

When the excess electron is captured by the modified radical adducts, the highest occupied molecular orbitals are in change order, as illustrated in Figure 4. For example, the singly occupied molecular orbital (SOMO) of TH3 is exclusively localized to the phosphate group, whereas the HOMO (the highest occupied molecular orbital) of the corresponding electron adduct is localized mainly on C2′. The net result from the excess negative charge is a delocalization to the neighboring C1′, which leads to the heterolytic dissociation of the *N*-glycosidic bond.

The above results point to the facts that the radical adducts of 5′dTMP−H or 5′dTMP−OH are incapable of inducing strand break or base release in DNA, in agreement with experimental findings.[31] Instead, their corresponding electron adducts, if formed, can contribute to DNA damage. It should be noted, however, that this will most likely require very low concentrations of molecular oxygen present. In a very recent paper, the heterolytic process of *N*-glycosidic bond cleavage in 2′-deoxyguanosine promoted by cations, especially by dicationic systems, were reported.[45] The BDE values in kcal/mol are 44.3 (singly protonated), 58.0 (Cu^+), −29.2 (Cu^{2+}), and −36.2 (doubly protonated). All results taken together illustrate that the decomposition is strongly dependent on the local DNA environments (electron attachment, proton transfer, metal ion, or radical stress) and on the stability of the decomposed species. Combined with the present results, the excess charges on DNA appear to always favor bond scission in the DNA molecule.

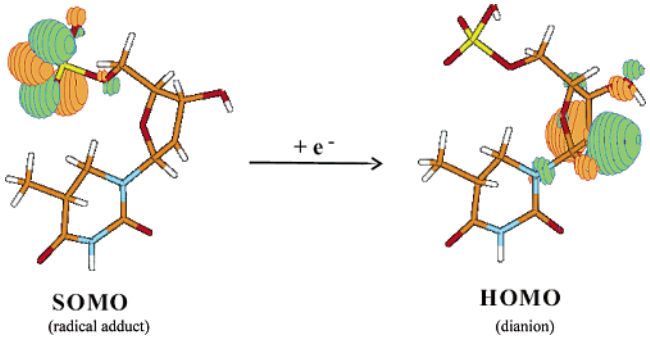

Figure 4. Highest occupied orbitals before and after addition of an excess electron to TH3.

According to the present studies, the rate-limiting step is exclusively determined by the H2′ proton-transfer reaction. The intramolecular proton-transfer rates for the electron adducts of 5′dTMP−H should be faster than the ones for the electronic adducts of 5′dTMP−OH given the lower barriers for the former. Furthermore, the DNA scission should be possible to observe for a system containing 5′dTMP−H electron adducts, albeit their formation as such consitute a minor process in cellular DNA.

3. Conclusions

In the present work, hybrid DFT methods have been employed to investigate the potential DNA-scission processes induced by H and OH radical addition to the C5 site of thymine and the subsequently reduced radical adducts in 5′dTMP. Geometries, NPA charges, electron affinities, and reaction energies were obtained at the B3LYP/6-31+G(d,p) level in gas phase, followed by energy calculations performed at the same level in solution ($\epsilon = 4.3$ and 78.4) using the IEF−PCM model. The barriers for H2′ abstraction by the C6 radical site in the radical adducts range from 25.1 to 35.1 kcal mol^{-1} in gas phase and 27.0 to 34.8 kcal mol^{-1} in aqueous solution, showing that the radical induced reactions are essentially prohibited.

Calculated electron affinities show that the capture of an excess electron by modified base radicals is favored by solvation also in nonaqueous medium, with the negative charges located on the radical-modified base and the phosphate fragments of ATH1(′) and ATOH1(′). Transfer of the H2′ proton occurs in the electron adducts of 5′dTMP−H and 5′dTMP−OH. The activation energies are 5.8 and 12.5 kcal mol^{-1} for the proton-transfer reactions in the electron adducts of 5′dTMP−H, whereas considerably higher barriers are predicted for the proton-transfer reactions in the electron adducts of 5′dTMP−OH. The barriers for subsequent cleavage of the *N*-glycosidic bonds are relatively low, from 0.1 to 1.6 kcal mol^{-1} at the B3LYP/6-31+G(d,p) level, and 5 ± 1.5 kcal mol^{-1} using the BB1K/6-31+G(d,p) method. The calculated bond dissociation energies (BDE) of the *N*-glycosidic bonds furthermore support the heterolytic bond cleavage and base release for all the reduced radical adducts.

The elongation of the *N*-glycosidic bond after the H2′ proton transfer reactions provide further support for the above conclusion. The bulk nonaqueous solvent plays a reverse effect on the proton transfer and the bond rupture, although the influence is too small to markedly influence the overall reaction pathways. Combined with previous work, excess charges (positive or negative) appear to have a significant effect in promoting DNA damage; the bond ruptures in the systems explored herein are controlled by the initial proton-transfer reactions from the sugar to the radical-modified base. The *N*-glycosidic bond dissociation (base release) is facilitated by the simultaneous formation of stable π-bonds between C1′−C2′ on the sugar and N1−C2 on the leaving base.

Acknowledgment. The Swedish Science Research Council (VR) is gratefully acknowledged for financial support. We also acknowledge generous grants of computing time at the National Supercomputing Facilities in Linköping (NSC) and Stockholm (PDC).

References and Notes

(1) von Sonntag, C.; Schuchman, H.-P. *Encyclopedia of Molecular Biology and Molecular Medicine*; VCH: Weinheim, 1996; Vol. 3.

(2) Dizdaroglu, M. *Mutat. Res.* **2005**, *591*, 45.

(3) Barker, S.; Weinfeld, M.; Murray, D. *Mutat. Res.* **2005**, *589*, 111.

(4) Halliwell, B.; Gutteridge, J. M. C. *Free Radicals in Biology and Medicine*; Oxford Science: Oxford, 1999.

(5) Lindahl, T.; Wood, R. D. *Science* **1999**, *286*, 1897.

(6) Stein, G.; Weiss, J. *Nature (London)* **1948**, *161*, 650.

(7) Commoner, B.; Townsend, J.; Pake, G. E. *Nature* **1954**, *174*, 689.

(8) von Sonntag, C. *The Chemical Basis of Radiation Biology*; Taylor & Francis: London, 1987.

(9) Wetmore, S. D.; Boyd, R. J.; Eriksson, L. A. *J. Phys. Chem. B* **1998**, *102*, 10602.

(10) Mundy, C. J.; Colvin, M. E.; Quong, A. A. *J. Phys. Chem. A* **2002**, *106*, 10063.

(11) Jena, N. R.; Mishra, P. C. *J. Phys. Chem. B* **2005**, *109*, 14205.

(12) Turecek, F.; Yao, C. *J. Phys. Chem. A* **2003**, *107*, 9221.

(13) Wetmore, S. D.; Boyd, R J.; Eriksson, L. A. *J. Phys. Chem. B* **1998**, *102*, 5369.

(14) Drew, H. R.; Wing, R. M.; Takano, T.; Broka, C.; Tanaka, S.; Itakura, K.; Dickerson, R. E. *Proc. Natl. Acad. Sci. U.S.A.* **1981**, *78*, 2179.

(15) Balasubramanian, B.; Pogozelski, W. K.; Tullius, T. D. *Proc. Natl. Acad. Sci. U.S.A.* **1998**, *95*, 9738.

(16) Boudaiffa, B.; Cloutier, P.; Hunting, D.; Huels, M. A.; Sanche, L. *Radiat. Res.* **2002**, *157*, 227.

(17) Zheng, Y.; Cloutier, P.; Hunting, D. J.; Wagner, J. R.; Sanche, L. *J. Am. Chem. Soc.* **2004**, *126*, 1002.

(18) Zheng, Y.; Cloutier, P.; Hunting, D. J.; Sanche, L.; Wagner, J. R. *J. Am. Chem. Soc.* **2005**, *127*, 16592.

(19) Boudaiffa, B.; Cloutier, P.; Hunting, D. J.; Huels, M. A.; Sanche, L. *Science* **2000**, *287*, 1658.

(20) Pan, X.; Cloutier, P.; Hunting, D. J.; Sanche, L. *Phys. Rev. Lett.* **2003**, *90*, 208102(4).

(21) Caron, L. G.; Sanche, L. *Phys. Rev. Lett.* **2003**, *91*, 113201(4).

(22) Gu, J.; Xie, Y.; Schaefer, H. F., III. *J. Am. Chem. Soc.* **2005**, *127*, 1053.

(23) Gu, J.; Xie, Y.; Schaefer, H. F., III. *J. Am. Chem. Soc.* **2006**, *128*, 1250.

(24) (a) Barrios, R.; Skurski, P.; Simons, J. *J. Phys. Chem. B* **2002**, *106*, 7991. (b) Berdys, J.; Anusiewicz, I.; Skurski, P.; Simons, J. *J. Phys. Chem. A* **2004**, *108*, 2999. (c) Anusiewicz, I.; Berdys, J.; Sobczyk, M.; Skurski, P.; Simons, J. *J. Phys. Chem. A* **2004**, *108*, 11381. (d) Berdys, J.; Anusiewicz, I.; Skurski, P.; Simons, J. *J. Am. Chem. Soc.* **2004**, *126*, 6441. (e) Berdys, J.; Skurski, P.; Simons, J. *J. Phys. Chem. B* **2004**, *108*, 5800. (f) Li, X.; Sevilla, M. D. Sanche, L. *J. Am. Chem. Soc.* **2003**, *125*, 13668.

(25) Lemaire, D. G. E.; Bothe, E.; Schulte-Frohlinde, D. *Int. J. Radiat. Biol.* **1984**, *45*, 351.

(26) Symons, M. C. R. *J. Chem. Soc., Faraday Trans.* **1987**, *83*, 1.

(27) Becker, D.; Sevilla, M. D. In *Advances in Radiation Biology*; DNA and Chromatin Damage Caused by Radiation, Vol. 17; Lett, J. T., Sinclair, W. K., Eds.; Academic Press: New York, 1987.

(28) Bothe, E.; Qureshi, G. A.; Schulte-Frohlinde, D. *Z. Naturforsch., C: Biosci.* **1983**, *38*, 1030.

(29) (a) Karam, L. R.; Dizdaroglu, M.; Simic, M. G. *Radiat. Res.* **1986**, *116*, 210. (b) Deeble, D. J.; von Sonntag, C. *Int. J. Radiat. Biol.* **1984**, *46*, 247.

(30) (a) Hildenbrand, K.; Behrens, G.; Schulte-Frohlinde, D.; Herak, J. N. *J. Chem.* Soc., *Perkin Trans. 2* **1989**, 283. (b) Schulte-Frohlinde, D.; Hildenbrand, K. In *Free Radicals in Synthesis and Biology;* Minisci, F., Ed.; Kluwer: Boston, 1989; p 335**.** (c) Schulte-Frohlinde, D.; Opitz, J.; Gomer, H.; Bothe, E. *Int. J. Radiat. Biol.* **1985**, *48*, 397. (d) Wagner, J. R.; van Lier, J. E.; Johnston, L. J. *Photochem. Photobiol.* **1990**, *52*, 333. (e) Krishna, C. M.; Decarroz, C.; Wagner, J. R.; Cadet, J.; Riesz, P. *Photochem. Photobiol.* **1987**, *46*, 175.

(31) Barvian, M. R.; Barkley, R. M.; Greenberg, M. M. *J. Am. Chem. Soc.* **1995**, *117*, 4894.

(32) Zhang, R. B.; Eriksson, L. A. to be published.

(33) Colson, A.-O.; Sevilla, M. D. *J. Phys. Chem.* **1995**, *99*, 13033

(34) Fujita, S.; Steenken, S. *J. Am. Chem. Soc.* **1981**, *103*, 2540.

(35) Zhang, Q.; Wang, Y. *J. Am. Chem. Soc.* **2004**, *126*, 13287.

(36) Dabkowska, I.; Rak, J.; Gutowski, M. *Eur. Phys. J. D* **2005**, *35*, 429.

(37) Becke, A. D. *J. Chem. Phys.* **1993**, *98*, 5648.

(38) Lee, C.; Yang, W.; Parr, R. G. *Phys. Rev. B* **1988**, *37*, 785.

(39) Reed, A. E.; Curtiss, L. A.; Weinhold, F. *Chem. Rev.* **1988**, *88*, 899.

(40) Tomasi, J.; Persico, M. *Chem. Rev.* **1994**, *94*, 2027.

(41) Frisch, M. J.; Trucks, G. W.; Schlegel, H. B.; Scuseria, G. E.; Robb, M. A.; Cheeseman, J. R.; Montgomery, J. A., Jr.; Vreven, T.; Kudin, K. N.; Burant, J. C.; Millam, J. M.; Iyengar, S. S.; Tomasi, J.; Barone, V.; Mennucci, B.; Cossi, M.; Scalmani, G.; Rega, N.; Petersson, G. A.; Nakatsuji, H.; Hada, M.; Ehara, M.; Toyota, K.; Fukuda, R.; Hasegawa, J.; Ishida, M.; Nakajima, T.; Honda, Y.; Kitao, O.; Nakai, H.; Klene, M.; Li, X.; Knox, J. E.; Hratchian, H. P.; Cross, J. B.; Bakken, V.; Adamo, C.; Jaramillo, J.; Gomperts, R.; Stratmann, R. E.; Yazyev, O.; Austin, A. J.; Cammi, R.; Pomelli, C.; Ochterski, J. W.; Ayala, P. Y.; Morokuma, K.; Voth, G. A.; Salvador, P.; Dannenberg, J. J.; Zakrzewski, V. G.; Dapprich, S.; Daniels, A. D.; Strain, M. C.; Farkas, O.; Malick, D. K.; Rabuck, A. D.; Raghavachari, K.; Foresman, J. B.; Ortiz, J. V.; Cui, Q.; Baboul, A. G.; Clifford, S.; Cioslowski, J.; Stefanov, B. B.; Liu, G.; Liashenko, A.; Piskorz, P.; Komaromi, I.; Martin, R. L.; Fox, D. J.; Keith, T.; Al-Laham, M. A.; Peng, C. Y.; Nanayakkara, A.; Challacombe, M.; Gill, P. M. W.; Johnson, B.; Chen, W.; Wong, M. W.; Gonzalez, C.; Pople, J. A. *Gaussian 03*, revision B.04; Gaussian, Inc.: Pittsburgh, PA, 2003.

(42) Becke, A. D. *Phys. Rev. A* **1988**, *38*, 3098; Becke, A. D. *J. Chem. Phys.* **1996**, *104*, 1040.

(43) Zhao, Y.; Gonzalez-Garcia, N.; Truhlar, D. G. *J. Phys. Chem. A* **2005**, *109*, 2012.

(44) Bernasconi, C. F.; Wenzel, P. J. *J. Org. Chem.* **2001**, *66*, 968.

(45) Ríos-Font, R.; Bertrán, J.; Rodríguez-Santiago, L.; Sodupe, M. *J. Phys. Chem. B* **2006**, *110*, 5767.